Hindawi
Mathematical Problems in Engineering
Volume 2021, Article ID 5286043, 14 pages
https://doi.org/10.1155/2021/5286043

Research Article

Stability Analysis and Chaos Control of Electronic Throttle Dynamical System

Shun-Chang Chang

Department of Mechanical and Automation Engineering, Da-Yeh University, No. 168, University Road, Dacun, Changhua 51591, Taiwan

Correspondence should be addressed to Shun-Chang Chang; changsc@mail.dyu.edu.tw

Received 29 July 2021; Revised 14 September 2021; Accepted 2 October 2021; Published 25 October 2021

Academic Editor: M. Syed Ali

This study addresses bifurcation analysis and controlling chaos in a vehicular electronic throttle. Using analysis techniques from nonlinear dynamics of an electronic throttle system based on bifurcation diagrams, we establish the existence of period-doubling and intermittency routes to chaos. The largest Lyapunov exponent is estimated from the synchronization to identify periodic and chaotic motions. Finally, the proposed continuous feedback control is employed to control chaos. To verify the effectiveness of the raised control strategy, we present a number of numerical simulations.

1. Introduction

In a conventional automotive engine, the throttle pedal is mechanically connected to the throttle body of the engine. In modern fuel injection systems, the throttle body is an essential part of the air intake system, controlling the flow of air into the engine to effectively combust fuel in the pistons. The correct amount of air is vital: too much or too little means that the engine cannot run smoothly [1]. The linkage mechanism between the throttle pedal and the throttle body can decrease engine efficiency. To maintain fuel efficiency and abide by emissions laws, fuel systems have been significantly changed in recent years. Most importantly, the linkage mechanism has been changed with an electronic module, widely known as an electronic throttle [2–5]. In automotive design, there are many advanced technologies of this concept which are in application already or in exploitation such as steering-by-wire, brake-by-wire, and throttle-by-wire [6]. The throttle-by-wire involves a pedal sensor, electronic throttle body, and an electronic control unit. Controlling the throttle valve opening angle adjusts air inflow into the engine. According to the demand of the engine, the amount of air flow will directly affect the performance of engine [7]. In electronic throttle, the throttle pedal is connected to the throttle body using a DC motor, which can enhance both the driving performance and fuel efficiency of the vehicle. This has encouraged its wide application in modern intelligent automobiles [8–11]. However, electronic throttle systems face two major problems: the nonlinear spring and the friction force in the valve [12]. Because electronic throttle valve systems feature many nonsmooth nonlinearities, the system is very hard to control [13–15]. Several studies have investigated nonlinear control for electronic throttle systems [16–20], which are typically depicted by a nonlinear dynamical system [13, 17]. Modifying one of these parameters alters the dynamics that exhibit chaos motion, leading to instability of engine running. Chaos appearing in electronic throttle system may lead to instability, resulting in engine misfire or incomplete combustion [21]. Modern nonlinear dynamics of bifurcation and chaos are widely employed in the research of nonlinear systems and many of these consider chaos dynamics in electronic throttle systems [22–24]. The initial condition sensitivity is one of the most important features of the chaotic system, and some related references about multistability and coexisting attractors are studied in recent years [25–28].

In this study, we employed numerical simulations such as bifurcation diagrams and Lyapunov exponents to indicate periodic and chaotic motions. The Lyapunov exponent can

be adopted to judge whether a system is in chaotic motion. The algorithms of Lyapunov exponents for smooth dynamic systems are well developed [29, 30]. However, there are some nonsmooth dynamic systems, such as dry friction and saturation, to which this algorithm cannot be applied directly. Several approaches are employed to calculate the largest Lyapunov exponents for nonsmooth dynamic systems [31–34]. In this paper, we employ the estimation scheme [31] for calculating the largest Lyapunov exponent of the electronic throttle system.

The dynamics of an electronic throttle system become unstable when it exhibits chaotic motion. Several practical engineering problems require control techniques to transform chaos into stable periodic motions. Various chaos control approaches have been proposed [36–41]. Improving the performance of an electronic throttle system necessitates transformation of chaotic motion into a steady-state periodic orbit. The purpose of transformation of chaos into a periodic motion is to raise the performance of an electronic throttle system. Our approach is based on the synchronization recommended by Kapitaniak [38] and Pyragas [39]. Numerical simulations confirm the effectiveness of the proposed procedure. Finally, adoption of Lyapunov stability theories guarantees the global stability of the nonlinear error system [42–44].

The paper is arranged as follows. Sections 2 and 3 describe the proposed model as well as the rich dynamics of an electronic throttle system. They are described employing numerical simulation methods. Section 4 explains the Lyapunov exponent used to decide whether the system exhibits chaos. A synchronization technique for chaos control in an electronic throttle system is presented in Section 5. The robustness of parametric perturbation in an electronic throttle system with synchronization control is depicted in Section 6. Conclusions and recommendations are listed in Section 7.

2. Problem Formulation

An outline of an electronic throttle system is presented in Figure 1, which is a mechatronic device. Because the DC motor is an acuter, it transmits torque to throttle shaft to control the air flow into the intake manifold [13].

The motor drive torque T_m is directly proportional to the current, which can be represented as follows:

$$T_m = k_m i(t), \tag{1}$$

where k_m is the motor torque coefficient.

The electrical device is modeled by induction L, resistance R, and an electromotive force $E = k_v\omega_m$ induced by rotation of the motor angle, where k_v is the motor counter electromotive coefficient and ω_m is the angular velocity of the motor rotor. The DC armature circuit equation is described as follows:

$$L\frac{di}{dt} + Ri = u(t) - k_v\omega_m(t), \tag{2}$$

where $u(t)$ is the applied voltage.

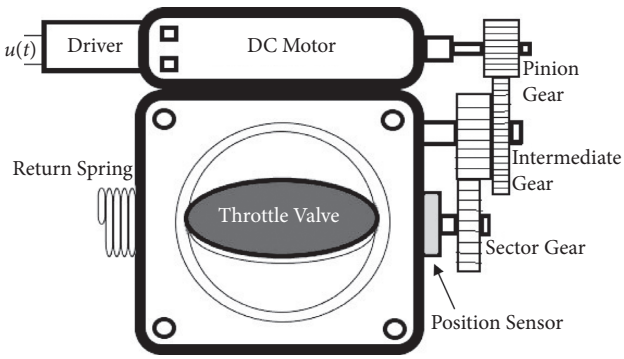

Figure 1: Outline of the electronic throttle system.

The nonlinear torque of the return spring can be described as follows:

$$T_s = k_s(\theta - \theta_0) + D\mathrm{sgn}(\theta - \theta_0), \tag{3}$$

where k_s is the spring coefficient, D is the spring compensation coefficient, θ is the throttle angle, and θ_0 is the initial throttle position (the so-called "limp-home" position).

Nonlinear friction torque is given by

$$T_f = k_d\omega(t) + k_f\mathrm{sgn}(\omega(t)), \tag{4}$$

where k_d is the viscous friction coefficient, k_f is the Coulomb friction coefficient, and ω is the throttle valve angular velocity.

If total inertia is J, according to equations (1)–(4), the resulting nonlinear model for the electronic throttle system is

$$J\frac{d\omega}{dt} = T_m - T_s - T_f \left[= k_m i - k_s(\theta - \theta_0) - D\mathrm{sgn}(\theta - \theta_0) - k_d\omega(t) - K_f\mathrm{sgn}(\omega(t)),\right. \tag{5a}$$

$$\frac{d\theta}{dt} = \omega(t) = N\omega_m(t). \tag{5b}$$

Taking into consideration equations (2)–(5) and denoting the state variable $x_1 = \theta - \theta_0$, $x_2 = \omega$, and $x_3 = i$, the state-space equations of electronic throttle can be rewritten as follows:

$$\dot{x_1} = x_2, \tag{6a}$$

$$\dot{x_2} = a_{21}x_1 + a_{22}x_2 + a_{23}x_3 - \alpha_1\mathrm{sgn}(x_1) - \alpha_2\mathrm{sgn}(x_2), \tag{6b}$$

$$\dot{x_3} = a_{32}x_2 + a_{33}x_3 + b_3u(t), \tag{6c}$$

where $a_{21} = -(k_s/J)$, $a_{22} = -(k_d/J)$, $a_{23} = (k_m/J)$, $\alpha_1 = (D/J)$, $\alpha_2 = (k_f/J)$, $a_{32} = -(k_v/NL)$, $a_{33} = -(R/L)$, $b_3 = (1/L)$, and $u = A_0\sin\tilde{\omega}t$.

For convenience, we first let $\omega_n = \sqrt{-a_{21}}$, $\Omega = (\tilde{\omega}/\omega_n)$, and $\tau = \omega_n t$ and then normalize equations (6a)–(6c) as follows:

$$\frac{dx_1}{d\tau} = x_2, \tag{7a}$$

$$\frac{dx_2}{d\tau} = x_1 + \frac{a_{22}}{\omega_n}x_2 + \frac{a_{23}}{{\omega_n}^2}x_3 - \frac{\alpha_1}{{\omega_n}^2}\operatorname{sgn}(x_1) - \frac{\alpha_2}{{\omega_n}^2}\operatorname{sgn}(x_2), \tag{7b}$$

$$\frac{dx_3}{d\tau} = \frac{a_{32}}{\omega_n}x_2 + \frac{a_{33}}{\omega_n}x_3 + \frac{b_3}{\omega_n}A_0\sin(\Omega\tau). \tag{7c}$$

The values of parameter for equation (7) are shown in Table 1 [45].

3. Structures in Bifurcation Diagram of Electronic Throttle System

We executed computer simulations based on equation (7) to explain the entire dynamics of the electronic throttle system. The commercial package was applied to solve the ordinary differential equation problems [46]. Here, initial conditions ($x_1(0) = 0.01$, $x_2(0) = -0.002$, and $x_3(0) = -0.005$) and time step (4×10^{-4}) are used. Figure 2 clearly reveals that the first period-doubling bifurcation occurred at about $\Omega = 1.619$ and that chaos arose below $\Omega = 1.582$. In order to detect period or chaos, we select a cross section $\sum$, where the flow "W" must be transverse to $\sum$. For point $(X_i, Y_i) \in \sum$, let t_0 be the time of next return to $\sum$. The map

$$P^{t_0}(X_i, Y_i) = (X_{i+1}, Y_{i+1}), \tag{8}$$

is the Poincaré map, as shown in Figure 3.

Figures 4–8 list the various dynamics displayed by this system in detail. Figures 4(a)–4(c) show the period-1 orbit with $\Omega > 1.619$. Also, Figures 5(a)–5(c) show a period-2 orbit at $\Omega = 1.595$. The first period-4 bifurcation occurred when Ω fell below 1.588. Figures 6(a)–6(c) show a period-4 orbit at $\Omega = 1.586$. The route to chaos via period-doubling bifurcations is obtained in Figure 2, resulting in a chatter that could create unstable behaviors, leading to incomplete combustion and eventually reducing engine performance. Strange attractors and continuous broad spectra are powerful indicators of chaos motion. Figures 7 and 8 reveal these characteristics of chaotic behavior.

4. Analysis of Chaotic Vibration Phenomena in Electronic Throttle System

The largest Lyapunov exponent is a powerful diagnostic technique for analysis of chaos. Any bounded motion in a system containing at least one positive Lyapunov exponent is defined as chaotic, and nonpositive Lyapunov exponents indicate periodic motion. In this paper, we estimated the largest Lyapunov exponent to verify the occurrence of chaos in an electronic throttle system. An easy method for estimating the largest Lyapunov exponent based on synchronization is recommended by Stefanski [31]. This way is described briefly as follows.

We consider a dynamic system comprising two identical n-dimensional subsystems:

Table 1: Parameter values for the simplified model.

Symbol	Parameter values
a_{21}	-1.6801×10^3
a_{22}	-32.9820
a_{23}	4.2941×10^3
a_{32}	-11.6039
a_{33}	-5.2087×10^2
α_1	4.6139×10^3
α_2	2.1073×10^3
b_3	4.7438×10^2
A_0	3.0

(i) A drive system:

$$\dot{x} = f(x). \tag{9}$$

(ii) A response system:

$$\dot{y} = f(y). \tag{10}$$

The response system (10) is combined with coupling coefficient d, and the drive system (9) remains the same. Therefore, the first-order differential equations can be rewritten as follows:

$$\begin{aligned} \dot{x} &= f(x), \\ \dot{y} &= f(y) + d(x - y). \end{aligned} \tag{11}$$

The qualification of synchronization is described in the following inequality:

$$d > \lambda_{\max}. \tag{12}$$

The least value of coupling coefficient d in synchronization d_s is estimated to be equal to the largest Lyapunov exponent as follows:

$$d_s = \lambda_{\max}. \tag{13}$$

We can apply equations (7) and (11) to create the following augmented system:

$$\frac{dx_1}{d\tau} = x_2, \tag{14a}$$

$$\frac{dx_2}{d\tau} = x_1 + \frac{a_{22}}{\omega_n}x_2 + \frac{a_{23}}{{\omega_n}^2}x_3 - \frac{\alpha_1}{{\omega_n}^2}\operatorname{sgn}(x_1) - \frac{\alpha_2}{{\omega_n}^2}\operatorname{sgn}(x_2), \tag{14b}$$

$$\frac{dx_3}{d\tau} = \frac{a_{32}}{\omega_n}x_2 + \frac{a_{33}}{\omega_n}x_3 + \frac{b_3}{\omega_n}A_0\sin(\Omega\tau), \tag{14c}$$

$$\frac{dy_1}{d\tau} = y_2 + d(x_1 - y_1), \tag{14d}$$

$$\frac{dy_2}{d\tau} = y_1 + \frac{a_{22}}{\omega_n}y_2 + \frac{a_{23}}{{\omega_n}^2}y_3 - \frac{\alpha_1}{{\omega_n}^2}\operatorname{sgn}(y_1) - \frac{\alpha_2}{{\omega_n}^2}\operatorname{sgn}(y_2) + d(x_2 - y_2), \tag{14e}$$

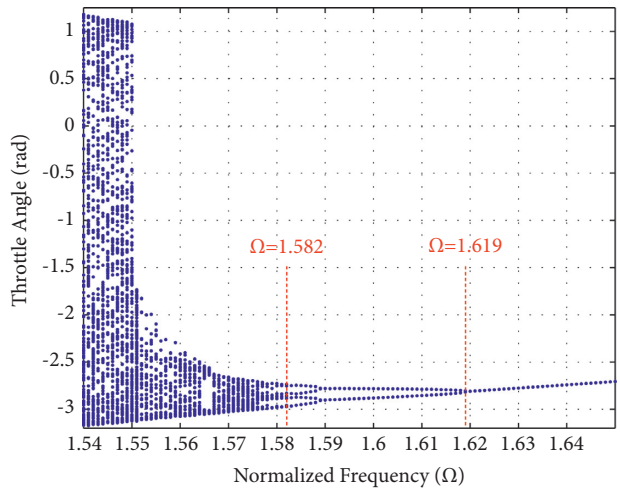

Figure 2: Bifurcation diagram of the throttle valve angle versus the normalized frequency, Ω.

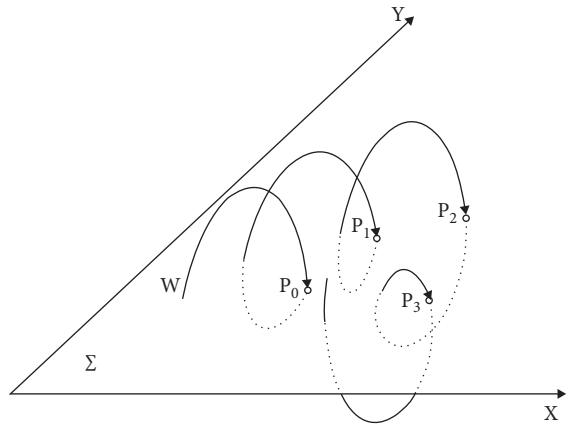

Figure 3: Illustration of a Poincaré section.

$$\frac{dy_3}{d\tau} = \frac{a_{32}}{\omega_n} y_2 + \frac{a_{33}}{\omega_n} y_3 + \frac{b_3}{\omega_n} A_0 \sin(\Omega\tau) + d(x_3 - y_3). \quad (14f)$$

We estimate the largest Lyapunov exponent in accordance with the above method. Figure 9 presents the estimated results. At $\mathbf{T_3}$, the sign of the largest Lyapunov exponent changed from negative to positive as Ω slowly decreased. At $\mathbf{T_{1\text{-}2}}$, the largest Lyapunov exponents became close to zero, beyond which the system could suffer bifurcation. The types of bifurcation have been described in the bifurcation diagram as presented in Figure 2. In a comparison of Figures 2 and 9, period-2 bifurcation is found at $\mathbf{T_1}$ and period-4 bifurcation is found at $\mathbf{T_2}$. All of the largest Lyapunov exponents are positive at $\Omega < 1.582$, representing chaotic motion.

5. Suppressing Chaos Based on Synchronization

Improving the performance of a dynamic system necessitates conversion of chaotic motion to a stable periodic orbit. Kapitaniak [38] and Pyragas [39] have proposed a simple and effective control method based on synchronization. This method relates the construction of a feedback in conjunction with a specific time-continuous perturbation. Figure 10 presents the feedback-controlled with an external periodic perturbation.

The method is described slightly as follows.

Consider the following n-dimensional systems:

$$\dot{p} = A(p), \quad (15)$$

$$\dot{q} = B(q) + F(t), \quad (16)$$

where $p(t)$, $q(t) \in R^n$ expresses the state vector and $F(t)$ is the input signal. Consider equation (16) exhibits chaos motion ($F(t) = 0$) and equation (15) shows periodic motion. A periodic system is expressed as the drive system, whereas a chaotic system is denoted as the response system. The block diagram of control strategy is presented in Figure 10. The difference between signals $q(t)$ and $p(t)$ is adopted as the control signal as follows:

$$F(t) = K[q(t) - p(t)], \quad (17)$$

where K denotes the feedback gain.

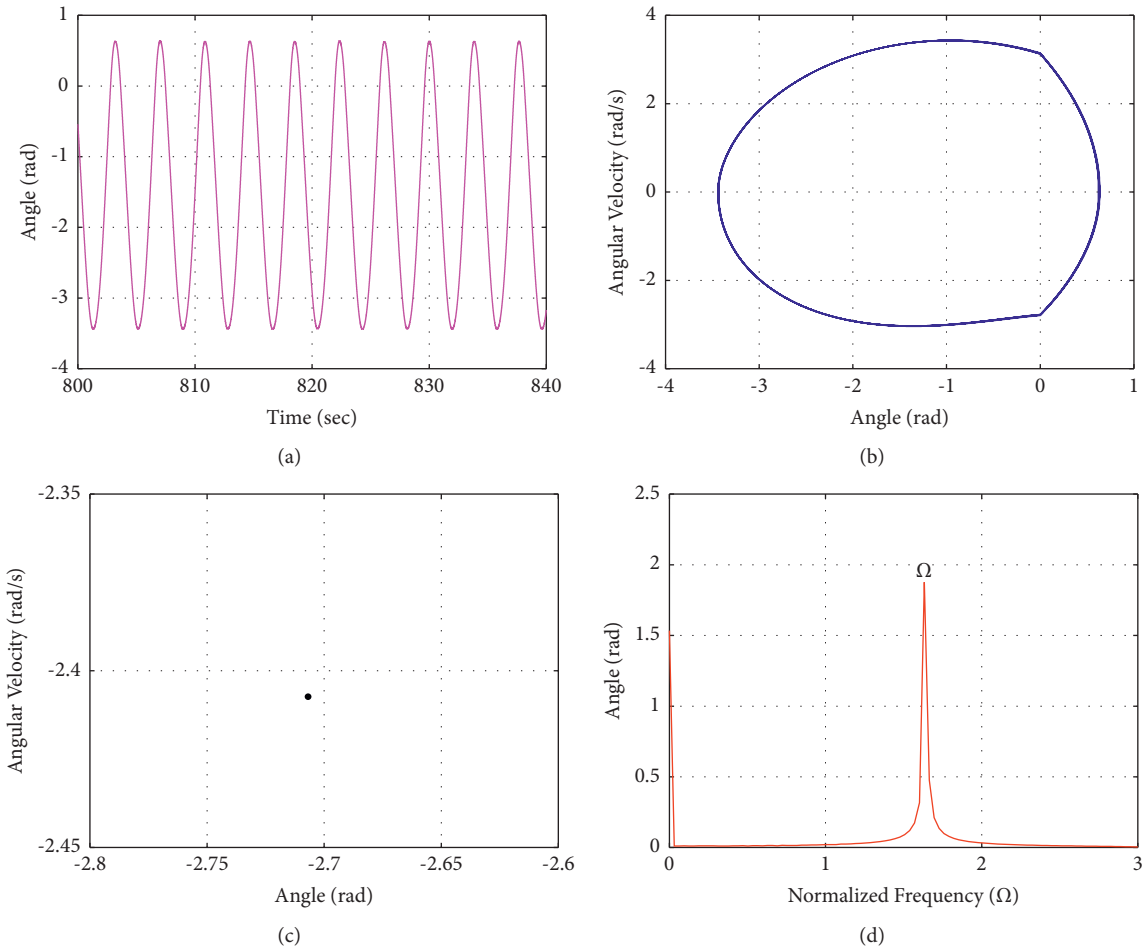

Figure 4: Period-1 motion at $\Omega = 1.64$: (a) time histories, (b) phase portraits, (c) Poincaré maps, and (d) power spectra.

When $\Omega_1 = 1.63$ in the drive system, equation (18) reveals period-1 motion:

$$\frac{dp_1}{d\tau} = p_2, \tag{18a}$$

$$\frac{dp_2}{d\tau} = p_1 + \frac{a_{22}}{\omega_n} p_2 + \frac{a_{23}}{\omega_n{}^2} p_3 - \frac{\alpha_1}{\omega_n{}^2}\operatorname{sgn}(p_1) - \frac{\alpha_2}{\omega_n{}^2}\operatorname{sgn}(p_2), \tag{18b}$$

$$\frac{dp_3}{d\tau} = \frac{a_{32}}{\omega_n} p_2 + \frac{a_{33}}{\omega_n} p_3 + \frac{b_3}{\omega_n} A_0 \sin(\Omega_1 \tau). \tag{18c}$$

When $\Omega_2 = 1.542$ in the response system, equation (19) suffers chaotic motion:

$$\frac{dq_1}{d\tau} = q_2, \tag{19a}$$

$$\frac{dq_2}{d\tau} = q_1 + \frac{a_{22}}{\omega_n} q_2 + \frac{a_{23}}{\omega_n{}^2} q_3 - \frac{\alpha_1}{\omega_n{}^2}\operatorname{sgn}(q_1) - \frac{\alpha_2}{\omega_n{}^2}\operatorname{sgn}(q_2), \tag{19b}$$

$$\frac{dq_3}{d\tau} = \frac{a_{32}}{\omega_n} q_2 + \frac{a_{33}}{\omega_n} q_3 + \frac{b_3}{\omega_n} A_0 \sin(\Omega_2 \tau). \tag{19c}$$

We introduced the control signal represented by equation (17) to equations (19a)–(19c) to synchronize equations (18) and (19). This yields the following coupled system:

$$\frac{dq_1}{d\tau} = q_2 + K(q_1 - p_1), \tag{20a}$$

$$\frac{dq_2}{d\tau} = q_1 + \frac{a_{22}}{\omega_n} q_2 + \frac{a_{23}}{\omega_n{}^2} q_3 - \frac{\alpha_1}{\omega_n{}^2}\operatorname{sgn}(q_1) - \frac{\alpha_2}{\omega_n{}^2}\operatorname{sgn}(q_2) + K(q_2 - p_2), \tag{20b}$$

$$\frac{dq_3}{d\tau} = \frac{a_{32}}{\omega_n} q_2 + \frac{a_{33}}{\omega_n} q_3 + \frac{b_3}{\omega_n} A_0 \sin(\Omega_2 \tau) + K(q_3 - p_3). \tag{20c}$$

Figure 11 expresses the bifurcation diagram, which clearly describes the dynamics of the system over a range of feedback gains. Specifically, chaos occurs in the region between $K = 0$ and $K = -1.0$, while period-1 occurs when K decreases below -1.0. When $K < -1.0$, equation (20) displays period-1 motion; that is, synchronization was achieved by a

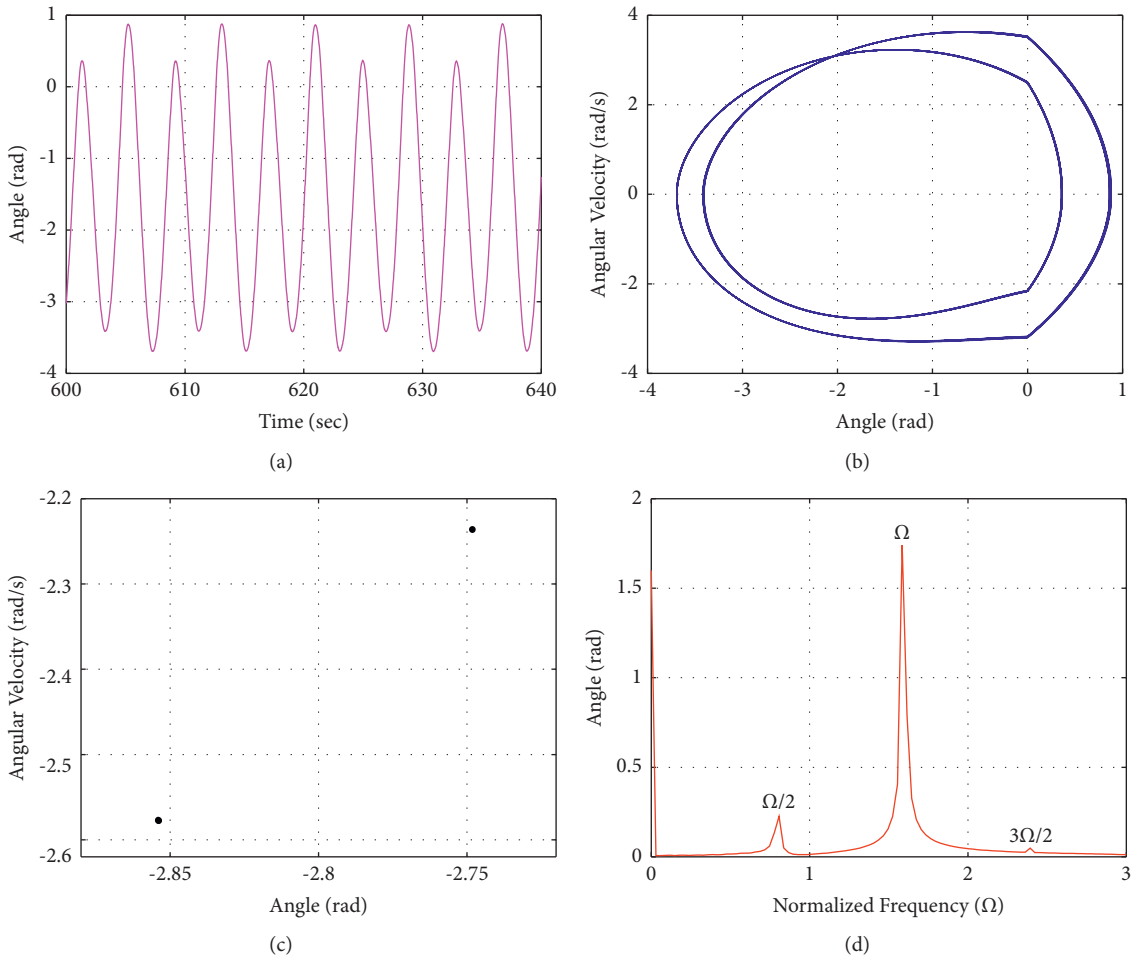

FIGURE 5: Period-2 motion at $\Omega = 1.595$: (a) time histories, (b) phase portraits, (c) Poincaré maps, and (d) power spectra.

control signal with $K < -1.0$. Transforming chaotic motion into period-1 for $K = -2.0$ and $\Omega = 1.542$ with synchronization control signal is introduced. Figure 12(a) plots the time histories of displacement in which the synchronization control signal is added after 60 s, Figure 12(b) reveals the phase portrait of the controlled system, and Figure 12(c) indicates the Poincaré map of the controlled system. Figure 13 shows the synchronization errors: $e_1 = q_1 - p_1$ and $e_2 = q_2 - p_2$. Zero synchronization errors indicate that synchronization has been achieved. This means that the control signal has successfully controlled chaotic motion to periodic orbit, thereby improving the chatter of the electronic throttle system. Obviously, the high-quality performance of the electronic throttle system could lead to improve vehicle drivability and fuel economy.

6. Study of Parametric Perturbations in Electronic Throttle System

We try to comprehend the effects of parameter errors on the performance of the synchronization control by adding a sinusoidal perturbation directly to parameters a_{22}, a_{23}, α_1, α_2, a_{32}, a_{33}, and b_3 in the drive system. If we assume that equation (18) denotes the drive system, then the corresponding controlled response system is as follows:

$$\dot{z}_1 = z_2 + u_1, \tag{21a}$$

$$\dot{z}_2 = z_1 + \frac{a_{22}(1 + \varepsilon \sin(\omega t))}{\omega_n} z_2 + \frac{a_{23}(1 + \varepsilon \sin(\omega t))}{\omega_n^2} z_3 - \frac{\alpha_1(1 + \varepsilon \sin(\omega t))}{\omega_n^2} \operatorname{sgn}(z_1) - \frac{\alpha_2(1 + \varepsilon \sin(\omega t))}{\omega_n^2} \operatorname{sgn}(z_2) + u_2, \tag{21b}$$

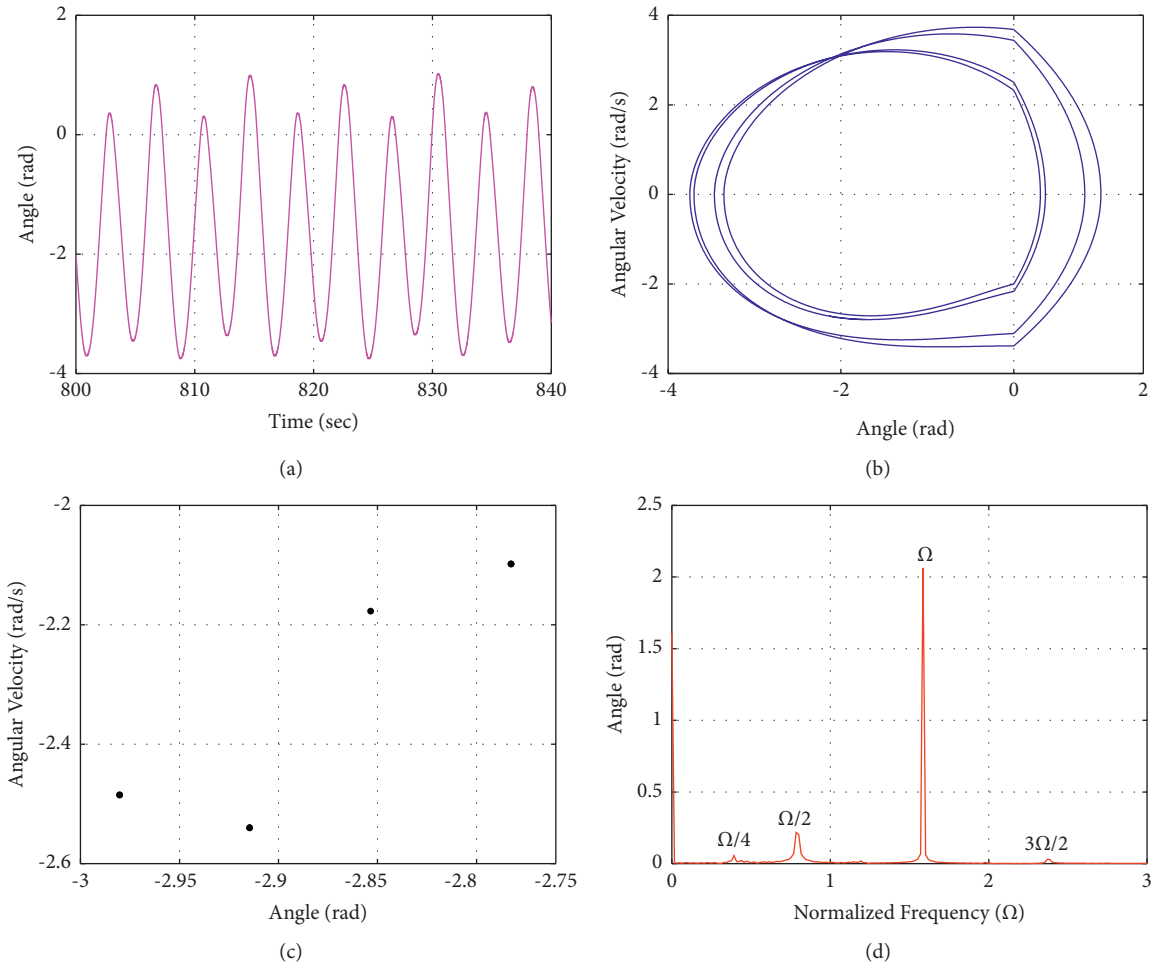

FIGURE 6: Period-4 motion at $\Omega = 1.586$: (a) time histories, (b) phase portraits, (c) Poincaré maps, and (d) power spectra.

$$\dot{z}_3 = \frac{a_{32}(1+\varepsilon\,\sin(\omega t))}{\omega_n} z_2 + \frac{a_{33}(1+\varepsilon\,\sin(\omega t))}{\omega_n} z_3 + \frac{b_3(1+\varepsilon\,\sin(\omega t))}{\omega_n} A_0 \sin(\Omega_1 \tau) + u_3, \tag{21c}$$

where ε is the amplitude of the perturbation and ω is the angular frequency.

Subtracting equation (18) from equations (21a)–(21c) we get the error equation as follows:

$$\dot{e}_1 = e_2 + u_1, \tag{22a}$$

$$\dot{e}_2 = e_1 + \frac{a_{22}\varepsilon\,\sin(\omega t)}{\omega_n} e_2 + \frac{a_{23}\varepsilon\,\sin(\omega t)}{\omega_n^{\,2}} e_3 - \frac{\alpha_1 \varepsilon \sin(\omega t)}{\omega_n^{\,2}} \operatorname{sgn}(e_1) - \frac{\alpha_2 \varepsilon\,\sin(\omega t)}{\omega_n^{\,2}} \operatorname{sgn}(e_2) + u_2, \tag{22b}$$

$$\dot{e}_3 = \frac{a_{32}\varepsilon\,\sin(\omega t)}{\omega_n} e_2 + \frac{a_{33}\varepsilon\,\sin(\omega t)}{\omega_n} e_3 + \frac{b_3 \varepsilon \sin(\omega t)}{\omega_n} A_0 \sin(\Omega_1 \tau) + u_3, \tag{22c}$$

where $e_1 = z_1 - p_1$, $e_2 = z_2 - p_2$, and $e_3 = z_3 - p_3$.

Considering a Lyapunov function of equation (22), we obtain the following:

$$V(e) = \frac{1}{2} e^T e. \tag{23}$$

The first derivative of $V(e)$ can be obtained as follows:

$$\dot{V}(e) = e_1 \dot{e}_1 + e_2 \dot{e}_2 + e_3 \dot{e}_3. \tag{24}$$

Therefore, if we select

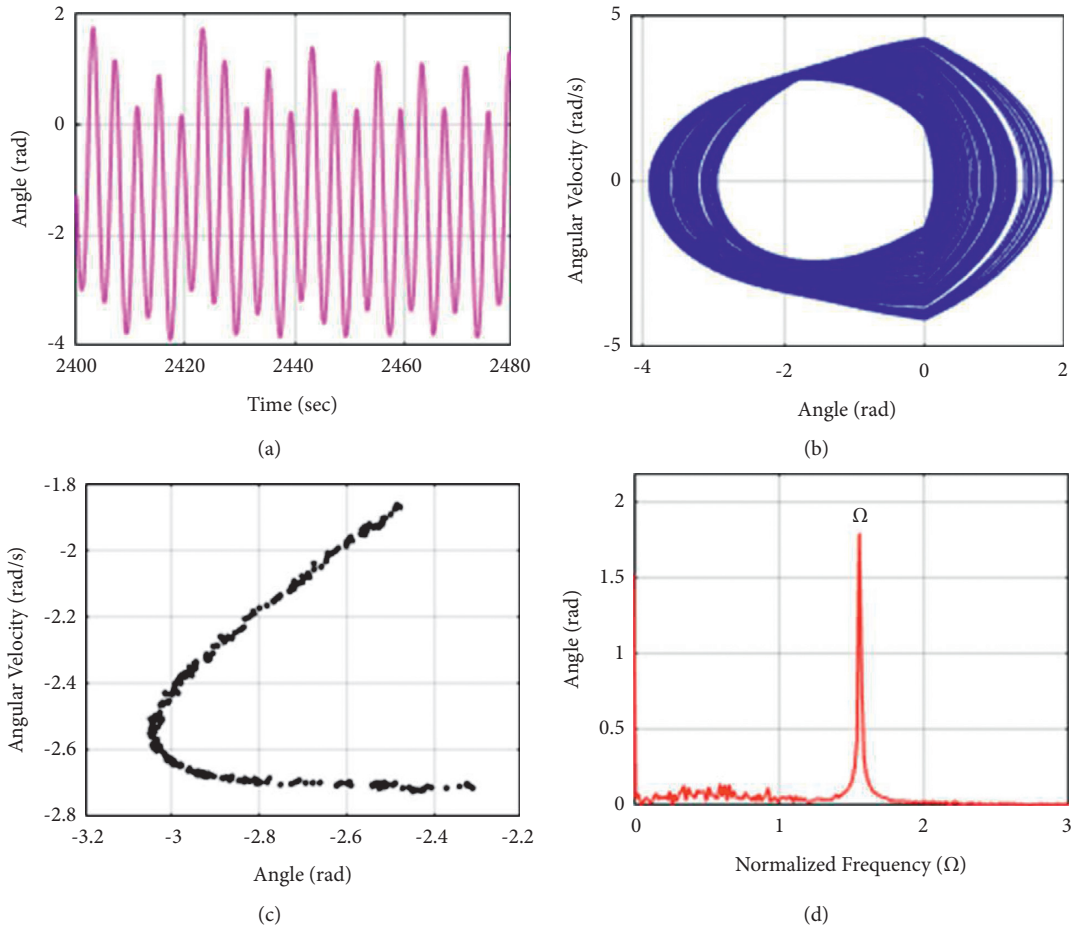

Figure 7: Chaotic motion at $\Omega = 1.56$: (a) time histories, (b) phase portraits, (c) Poincaré maps, and (d) power spectra.

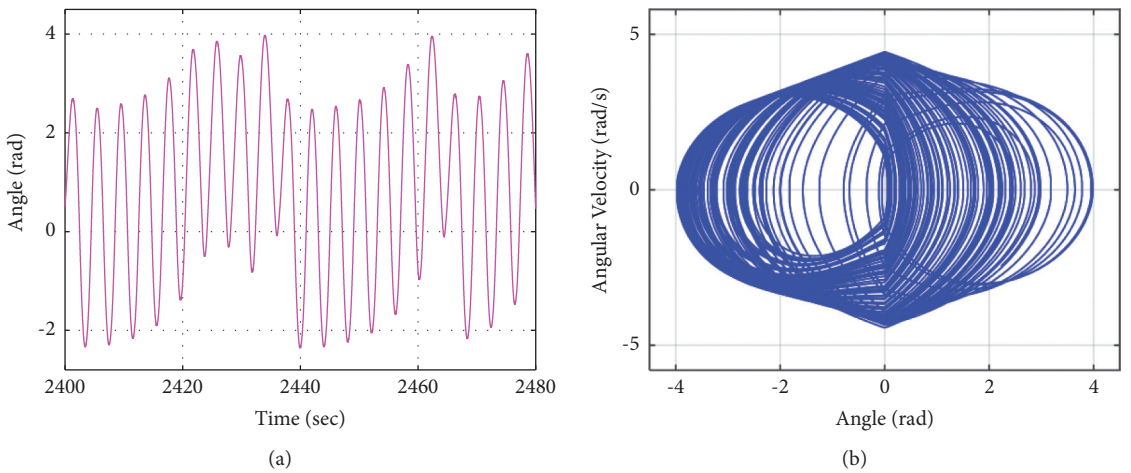

Figure 8: Continued.

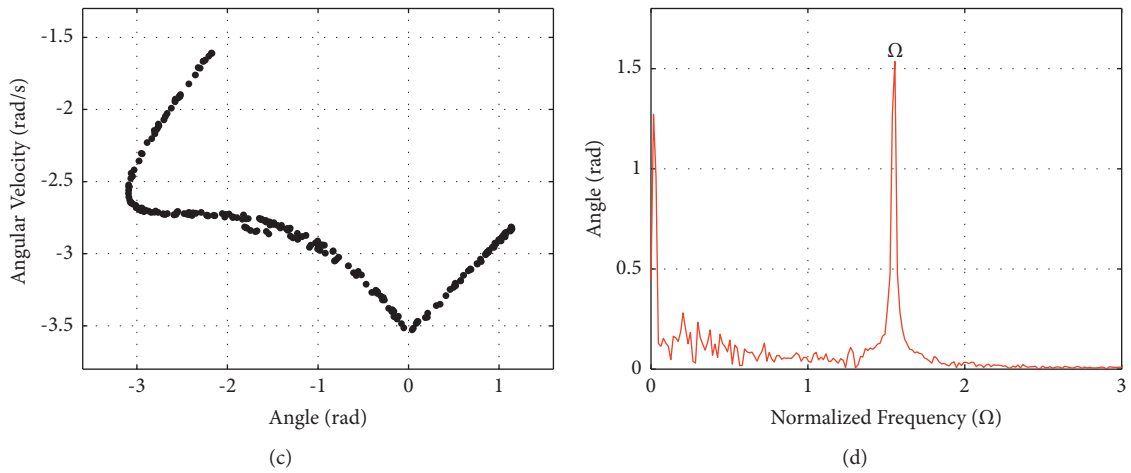

Figure 8: Chaotic motion at $\Omega = 1.548$: (a) time histories, (b) phase portraits, (c) Poincaré maps, and (d) power spectra.

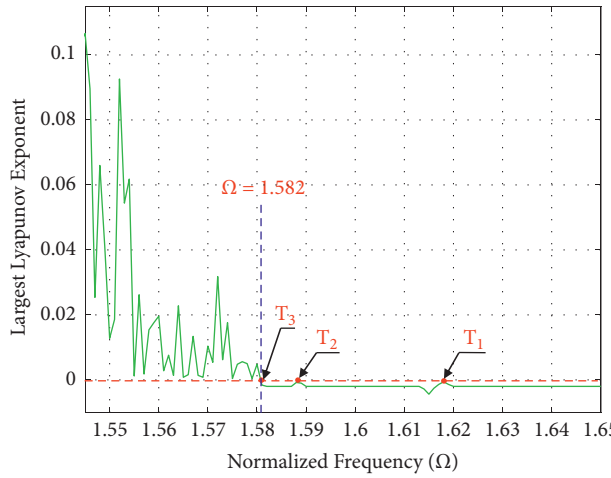

Figure 9: Estimation of the maximal Lyapunov exponent versus Ω.

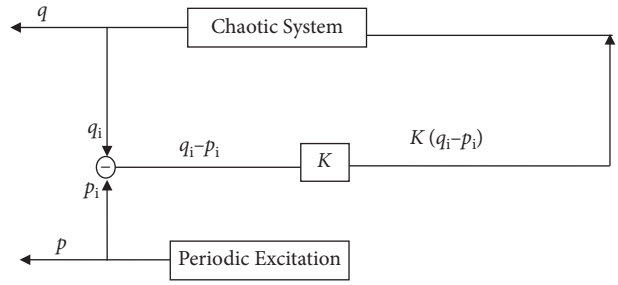

Figure 10: Block diagram of the synchronization method.

$$u_1 = -e_1 - e_2, \tag{25a}$$

$$u_2 = -e_1 - e_2 - \frac{a_{22}\varepsilon \sin(\omega t)}{\omega_n} e_2 - \frac{a_{23}\varepsilon \sin(\omega t)}{\omega_n^2} e_3 + \frac{\alpha_1 \varepsilon \sin(\omega t)}{\omega_n^2} \operatorname{sgn}(e_1) + \frac{\alpha_2 \varepsilon \sin(\omega t)}{\omega_n^2} \operatorname{sgn}(e_2), \tag{25b}$$

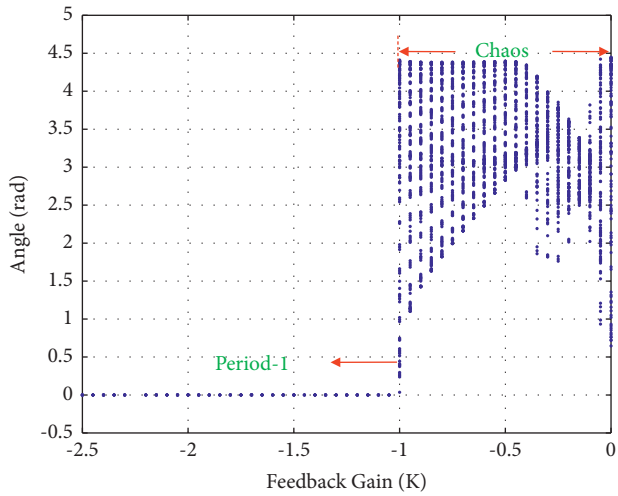

Figure 11: Bifurcation diagram of throttle valve angle against K for the electronic throttle system with synchronization.

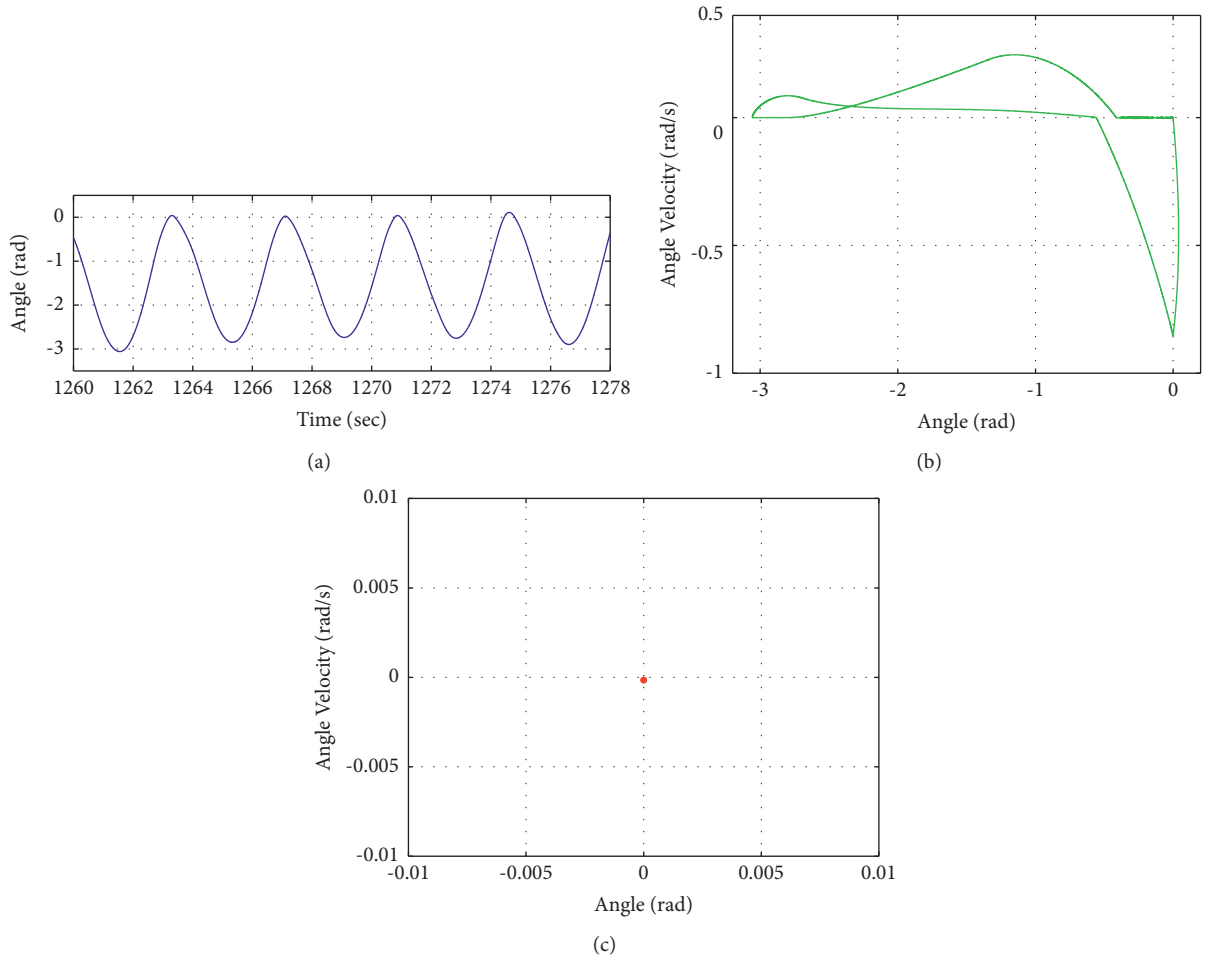

Figure 12: Controlling chaos ($\Omega = 1.542$) to a desired period-1 with synchronization control signal at $K = -2.0$: (a) time histories of the controlled system, (b) phase portrait of the controlled system, and (c) Poincaré map of the controlled system.

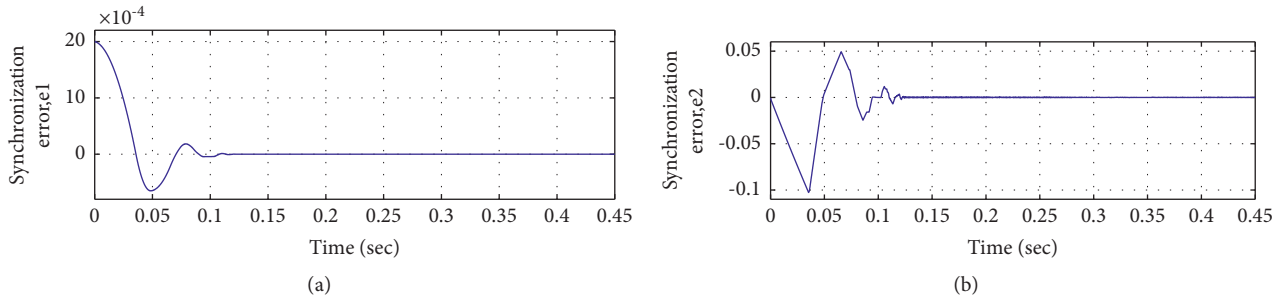

Figure 13: Synchronization errors at $K = -2.0$.

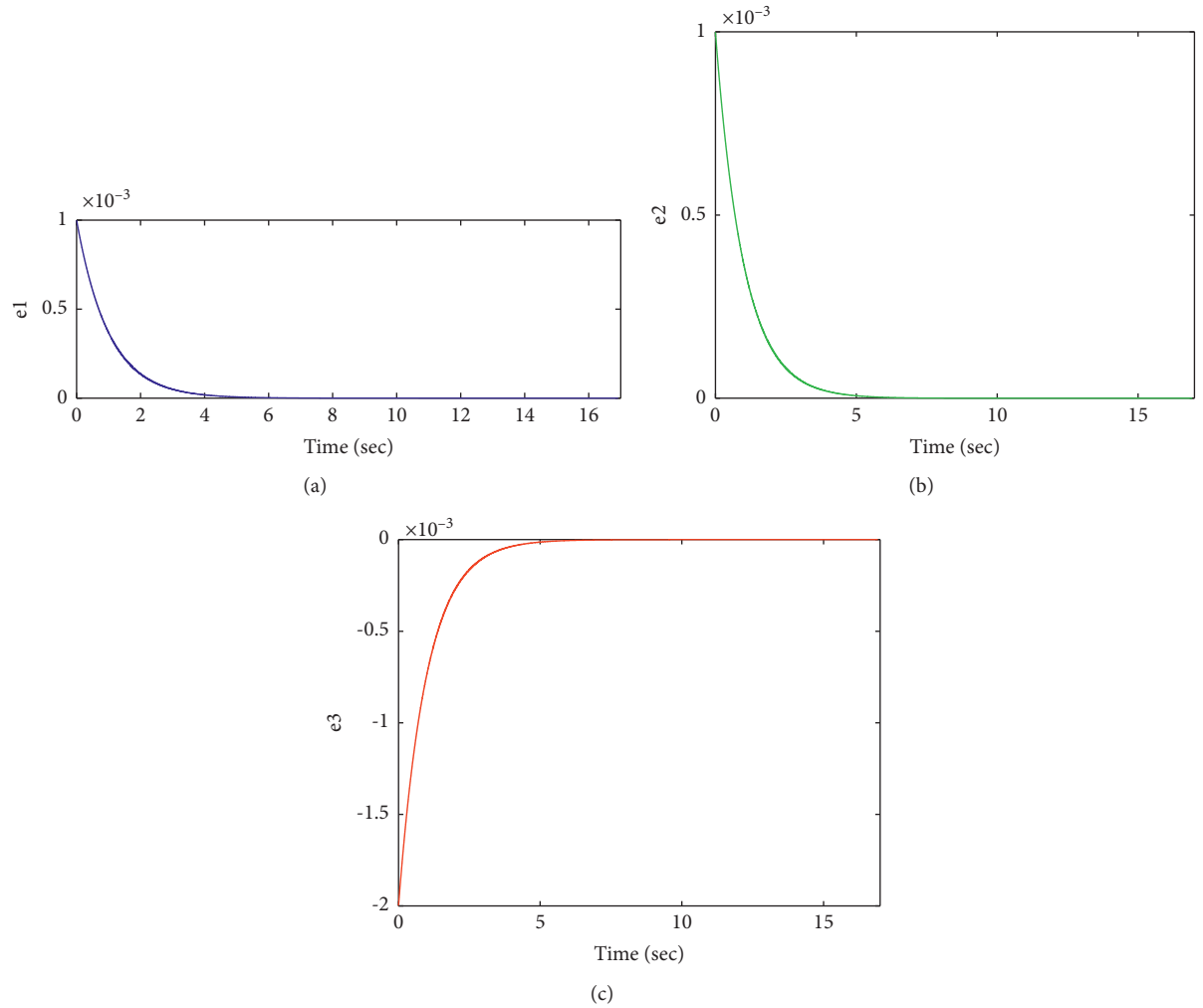

Figure 14: Dynamic errors of synchronization for drive and response systems: (a) $e_1 = z_1 - x_1$, (b) $e_2 = z_2 - x_2$, and (c) $e_3 = z_3 - x_3$.

$$u_3 = -e_3 - \frac{a_{32}\varepsilon \sin(\omega t)}{\omega_n} e_2 - \frac{a_{33}\varepsilon \sin(\omega t)}{\omega_n} e_3 - \frac{b_3 \varepsilon \sin(\omega t)}{\omega_n} A_0 \sin(\Omega_1 \tau), \tag{25c}$$

then

$$\dot{V}(e) = -e_1^2 - e_2^2 - e_3^2, \tag{26}$$

and $\dot{V}(e) < 0$ is completed. Since $\dot{V}(e)$ is a negatively defined function, the error states are $\lim_{t \longrightarrow \infty} \|e(t)\| = 0$. Thus, the

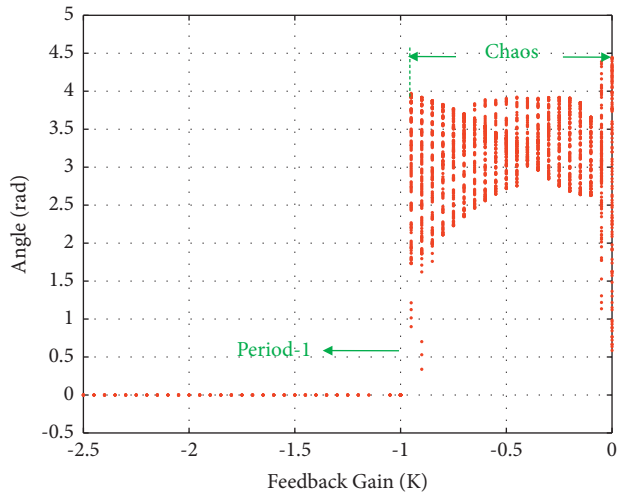

FIGURE 15: Bifurcation diagram with synchronization under perturbed parameters: $a_{22} + a_{22}\varepsilon\sin\omega t$, $a_{23} + a_{23}\varepsilon\sin\omega t$, $\alpha_1 + \alpha_1\varepsilon\sin\omega t$, $\alpha_2 + \alpha_2\varepsilon\sin\omega t$, $a_{32} + a_{32}\varepsilon\sin\omega t$, $a_{33} + a_{33}\varepsilon\sin\omega t$, and $b_3 + b_3\varepsilon\sin\omega t$.

states of the controlled response and drive systems are synchronized globally and asymptotically [47].

We evaluated these theoretical results using simulations with perturbation parameters: $\varepsilon = 0.01$ and ω =125.6 rad/s. Figures 14(a)–14(c) present dynamics of synchronization errors, for example, $e_1 = z_1 - p_1$, $e_2 = z_2 - p_2$, and $e_3 = z_3 - p_3$. The synchronization error eventually approaches to zero, resulting in stabilization of the error system. In other words, the proposed control method is robust to parameter mismatch in the electronic throttle system. Figure 15 illustrates the effects of parametric perturbation. Therefore, if chaos is converted into period-1, then feedback gain would be picked to the region $K \leq -1.0$. Again, the proposed control method was shown to suppress chaos under these perturbed parameters (e.g., a_{22}, a_{23}, α_1, α_2, a_{32}, a_{33}, and b_3) using equation (18).

7. Conclusions

This study examined rich nonlinear dynamics and developed a valid approach for controlling chaos in an electronic throttle system. The bifurcation diagram showed many nonlinear dynamics, indicating that the electronic throttle system appeared chaos under lower Ω. We adopt numerical simulations, such as phase portraits, Poincaré maps, and frequency spectra, to explore the nonlinear dynamics of the system in detail. The Lyapunov exponent is a strong analysis tool for determining whether an electronic throttle system exhibits chaotic motion. We estimated the largest Lyapunov exponent based on synchronization properties. Then, we applied a continuous feedback control method based on synchronization to control chaos and prevent chatter phenomena of the electronic throttle system.

Other many chaos control methods have been derived, such as synchronization, feedback control, neuro-fuzzy control, and adaptive control. In this study, a continuous feedback control method based on synchronization was adopted to control the chaos of an electronic throttle system. The effectiveness of the proposed chaos control method was verified by numerical simulations. In general, it is found that compared with other chaos control methods, the synchronization control strategy is simple and easy to control chaos. Finally, we adopt bifurcation diagram and Lyapunov stability theory to reveal the robustness of parametric perturbation in an electronic throttle system under synchronization control. We believe that an in-depth understanding of the nonlinear dynamics and chaos control for an electronic throttle system will help to promote intelligent vehicles.

Data Availability

No data were used to support this study as our results were based on simulation.

Conflicts of Interest

The author declares that there are no conflicts of interest for this published paper.

Acknowledgments

The author gratefully acknowledges the support of the Ministry of Science and Technology of Taiwan, R.O.C. under grant no. MOST 108-2221-E-212-010-MY3.

References

[1] D. Song and Y. Li, "Study on composite control strategy of transient air-fuel ratio for gasoline engine based on model," *IOP Conference Series: Earth and Environmental Science*, vol. 513, no. 1, pp. 012027–012033, 2020.

[2] M. N. Dolly and V. D. Kevala, "Design of diagnosis device for electronic throttle body," *International Research Journal of Engineering and Technology*, vol. 6, no. 6, pp. 2817–2819, 2019.

[3] M. Mcharek, T. Azib, M. Hammadi, C. Larouci, and J. Y. Choley, "Multiphysical design approach for automotive electronic throttle body," *IEEE Transactions on Industrial Electronics*, vol. 67, no. 8, pp. 6752–6761, 2019.

[4] L. Acho, G. Pujol-Vázquez, and J. Gibergans-Báguena, "A recent electronic control circuit to a throttle device," *Electronics*, vol. 9, no. 1, pp. 191–201, 2020.

[5] Y. Qin and H. Wang, "Analytical framework of string stability of connected and autonomous platoons with electronic throttle angle feedback," *Transportmetrica A: Transportation Science*, vol. 17, no. 1, pp. 59–80, 2021.

[6] H. Hafez, S. A. Maged, and M. Abdelaziz, "Modular design of x-by-wire systems to facilitate autonomous platform development," in *Proceedings of the 8th IEEE International Conference on Control, Mechatronics and Automation (ICCMA)*, pp. 42–46, Moscow, Russia, November 2020.

[7] S. AhmedAl-Samarraie and Y. Khudhair Abbas, "Design of electronic throttle valve position control system using nonlinear PID controller," *International Journal of Computer Applications*, vol. 59, no. 15, pp. 27–34, 2012.

[8] A. K. Yadav, P. Gaur, and S. Tripathi, "Design and control of an intelligent electronic throttle control system," in *Proceedings of the IEEE International Conference on Energy Economics and Environment (ICEEE)*, pp. 1–5, Greater Noida, India, March 2015.

[9] M. Afify, A. S. Abuabed, and N. Alsbou, "Smart engine speed control system with ECU system interface," in *Proceedings of the IEEE International Instrumentation and Measurement Technology Conference (I2MTC)*, pp. 1–6, Houston, TX, USA, May 2018.

[10] L. Chen, Y. Zhang, K. Li, Q. Li, and Q. Zheng, "Car-following model of connected and autonomous vehicles considering both average headway and electronic throttle angle," *Modern Physics Letters B*, vol. 35, no. 15, Article ID 2150257, 2021.

[11] J. Xue and X. Jiao, "Speed cascade adaptive control for hybrid electric vehicle using electronic throttle control during car-following process," *ISA Transactions*, vol. 110, pp. 328–343, 2021.

[12] C. H. Chen, H. L. Tsai, and Y. S. Lin, "Servo control design for electronic throttle valve with nonlinear spring effect," in *Proceedings of the 11th IEEE International Workshop on Advanced Motion Control (AMC)*, pp. 88–93, Nagaoka, Japan, March 2010.

[13] Q. Zeng and J. Wan, "Nonlinear PID control of electronic throttle valve," in *Proceedings of the IEEE International Conference on Electrical and Control Engineering*, pp. 722–724, Yichang, China, September 2011.

[14] A. Jansri, T. Pongsuttiyakorn, and P. Sooraksa, "On practical control of electronic throttle body," in *Proceedings of the 9th IEEE International Conference on Fuzzy Systems and Knowledge Discovery*, pp. 349–351, Chongqing, China, May 2012.

[15] M. Ye and H. Wang, "A robust adaptive chattering-free sliding mode control strategy for automotive electronic throttle system via genetic algorithm," *IEEE Access*, vol. 8, pp. 68–80, 2019.

[16] R. Loh, W. Thanom, J. Pyko, and A. Lee, "Electronic throttle control system: modeling, identification and model-based control designs," *Engineering*, vol. 5, no. 7, pp. 587–600, 2013.

[17] A. Humaidi and A. Hameed, "Design and comparative study of advanced adaptive control schemes for position control of electronic throttle valve," *Information*, vol. 10, no. 2, pp. 65–79, 2019.

[18] Z. Sun and X. Jiao, "Adaptive prescribed performance servo control of an automotive electronic throttle system with actuator constraint," *Turkish Journal of Electrical Engineering & Computer Sciences*, vol. 28, no. 2, pp. 956–968, 2020.

[19] Z. Cao, Y. Niu, and H. R. Karimi, "Sliding mode control of automotive electronic valve system under weighted try-once-discard protocol," *Information Sciences*, vol. 515, no. 5, pp. 324–340, 2020.

[20] D. Wang, S. Liu, Y. He, and J. Shen, "Barrier Lyapunov function-based adaptive back-stepping control for electronic throttle control system," *Mathematics*, vol. 9, no. 4, pp. 326–340, 2021.

[21] P. Boguś, J. Merkisz, R. Grzeszczyk, and S. Mazurek, "Nonlinear analysis of combustion engine vibroacoustic signals for misfire detection," *SAE Technical Paper*, 2003.

[22] D. Passaquay, S. Boverie, G. Heredia, A. Ollero, A. Titli, and J. Aracil, "Fuzzy modelling, control and stability analysis of an automotive engine," *IFAC Proceedings Volumes*, vol. 34, no. 1, pp. 223–228, 2001.

[23] I.-S. Yang, M.-G. Song, and D.-I. Lee, "Nonlinear dynamic inversion based control for electronic throttle," *Transactions of the Korean Society of Automotive Engineers*, vol. 20, no. 2, pp. 8–14, 2012.

[24] W. Ren, R. Cheng, and H. Ge, "Bifurcation analysis for a novel heterogeneous continuum model considering electronic throttle angle changes with memory," *Applied Mathematics and Computation*, vol. 401, Article ID 126079, 2021.

[25] N. Wang, G. Zhang, and H. Bao, "Bursting oscillations and coexisting attractors in a simple memristor-capacitor-based chaotic circuit," *Nonlinear Dynamics*, vol. 97, no. 2, pp. 1477–1494, 2019.

[26] N. Wang, G. Zhang, N. V. Kuznetsov, and H. Bao, "Hidden attractors and multistability in a modified Chua's circuit," *Communications in Nonlinear Science and Numerical Simulation*, vol. 92, Article ID 105494, 2021.

[27] N. Wang, G. Zhang, and H. Bao, "A simple autonomous chaotic circuit with dead-zone nonlinearity," *IEEE Transactions on Circuits and Systems II: Express Briefs*, vol. 67, no. 12, pp. 3502–3506, 2020.

[28] N. Wang, C. Li, H. Bao, M. Chen, and B. Bao, "Generating multi-scroll chua's attractors via simplified piecewise-linear chua's diode," *IEEE Transactions on Circuits and Systems I: Regular Papers*, vol. 66, no. 12, pp. 4767–4779, 2019.

[29] A. Wolf, J. B. Swift, H. L. Swinney, and J. A. Vastano, "Determining Lyapunov exponents from a time series," *Physica D: Nonlinear Phenomena*, vol. 16, no. 3, pp. 285–317, 1985.

[30] G. Benettin, L. Galgani, A. Giorgilli, and J.-M. Strelcyn, "Lyapunov characteristic exponents for smooth dynamical systems and for Hamiltonian systems; a method for computing all of them. Part 2: numerical application," *Meccanica*, vol. 15, no. 1, pp. 21–30, 1980.

[31] A. Stefanski, "Estimation of the largest Lyapunov exponent in systems with impacts," *Chaos, Solitons & Fractals*, vol. 11, no. 15, pp. 2443–2451, 2000.

[32] J. Kang, "Calculation of Lyapunov exponents in impacted beam on distributed contact," *Journal of Sound and Vibration*, vol. 431, no. 8, pp. 295–303, 2018.

[33] W. Ma, W. Song, and L. Qiu, "Instability analysis of pressure relief valve based on Lyapunov exponent and non-smooth bifurcation theory," *Journal of Applied Science and Engineering*, vol. 22, no. 2, pp. 329–336, 2019.

[34] M. Balcerzak, A. Dabrowski, B. Blazejczyk–Okolewska, and A. Stefanski, "Determining Lyapunov exponents of non-smooth systems: perturbation vectors approach," *Mechanical Systems and Signal Processing*, vol. 141, Article ID 106734, 2020.

[35] E. Ott, C. Grebogi, and J. A. Yorke, "Controlling chaos," *Physical Review Letters*, vol. 64, no. 11, pp. 1196–1199, 1990.

[36] H. Gritli and S. Belghith, "Bifurcations and chaos in the semi-passive bipedal dynamic walking model under a modified OGY-based control approach," *Nonlinear Dynamics*, vol. 83, no. 4, pp. 1955–1973, 2016.

[37] H. Gritli and S. Belghith, "Walking dynamics of the passive compass-gait model under OGY-based control: emergence of bifurcations and chaos," *Communications in Nonlinear Science and Numerical Simulation*, vol. 47, pp. 308–327, 2017.

[38] T. Kapitaniak, "Continuous control and synchronization in chaotic systems," *Chaos, Solitons & Fractals*, vol. 6, pp. 237–244, 1995.

[39] K. Pyragas, "Continuous control of chaos by self-controlling feedback," *Physics Letters A*, vol. 170, no. 6, pp. 421–428, 1992.

[40] X. Yi, R. Guo, and Y. Qi, "Stabilization of chaotic systems with both uncertainty and disturbance by the UDE-based control method," *IEEE Access*, vol. 8, pp. 62471–62477, 2020.

[41] S. C. Chang, "Stability, chaos detection, and quenching chaos in the swing equation system," *Mathematical Problems in Engineering*, vol. 2020, Article ID 6677084, 2020.

[42] M. Rafikov and J. M. Balthazar, "On an optimal control design for Rössler system," *Physics Letters A*, vol. 333, no. 3-4, pp. 241–245, 2004.

[43] M. Rafikov and J. M. Balthazar, "On control and synchronization in chaotic and hyperchaotic systems via linear feedback control," *Communications in Nonlinear Science and Numerical Simulation*, vol. 13, no. 7, pp. 1246–1255, 2008.

[44] M. Rafikov, J. M. Balthazar, and A. M. Tusset, "An optimal linear control design for nonlinear systems," *Journal of the Brazilian Society of Mechanical Sciences and Engineering*, vol. 30, no. 4, pp. 279–284, 2008.

[45] Y. Pan, U. Ozguner, and O. H. Dagci, "Variable-structure control of electronic throttle valve," *IEEE Transactions on Industrial Electronics*, vol. 55, no. 11, pp. 3899–3907, 2008.

[46] IMSL, Inc., *User's Manual–IMSL Math/Library*, IMSL, Inc., Houston, TX, USA, 1989.

[47] H. K. Khalil, *Nonlinear Systems*, Prentice-Hall, Hoboken, NJ, USA, Third edition, 2002.